ELSEVIER

Journal of Hazardous Materials 55 (1997) 93–107

JOURNAL OF HAZARDOUS MATERIALS

Mathematical modeling of hexavalent chromium decontamination from low surface charged soils

Bala S. Haran, Branko N. Popov *, Guanghong Zheng, Ralph E. White

Department of Chemical Engineering, University of South Carolina, Columbia, SC 29208, USA

Abstract

A new electrokinetic technology has been developed for in-situ decontamination of hexavalent chromium in sand. Imposition of a constant potential gradient across the soil matrix through a graphite cathode and iron anode resulted in successful migration of chromate towards the anode. The hexavalent chromium ions are reduced to the harmless trivalent form by chemical reaction with the anodic electrochemical dissolution product, Fe^{2+}. The alkaline front generated at the cathode due to water reduction flushes across the cell and favors faster transport of chromate by enhancing its conductivity. The acidic front generated due to water oxidation at the anode remains adjacent at the electrode–sand interface due to its consumption by the corrosion reaction with iron. The lower production rate of H^+ is also due to the competing anodic dissolution reaction. The low pH at the anodic region favors the reduction of hexavalent chromium to its trivalent state. The experimental results are compared with a theoretical model developed from first principles. The water electrolysis reactions at both electrodes, the sorption processes in sand and the water hydrolysis reaction have been included in the model. Concentration profiles for the movement of ionic species under a potential field were simulated for different times. The model predicts the sweep of the alkaline front across the cell due to the transport of OH^- ions. Comparison of the chromate concentration profiles with experimental data after 28 days of electrolysis shows good agreement. The potassium cations are positively charged and remained at the cathode where they had been placed initially. The good agreement between the model and the data demonstrates that the analysis is likely to be an accurate estimation of the physical situation, within the limits of the assumptions made. © 1997 Elsevier Science B.V.

Keywords: Simulation; Surface charge; Electro-migration; Alkaline front

* Corresponding author. Tel.: +1 803 7777314; fax: +1 803 7778265.

PII S0304-3894(97)00009-5

1. Introduction

Contamination of soils and ground water by hazardous wastes is a widespread problem that constitutes a serious threat to public health. During the past decade, the need to develop cost effective and efficient techniques for remediation of large tracts of contaminated soil has grown. Most of the existing technologies are applicable only to soils of high hydraulic conductivity. Electro-kinetics offers the possibility of transport and in-situ remediation of contaminants in cases where conventional techniques are not feasible [1,2].

Electro-osmosis and ionic migration form the dominant transport mechanisms in the electrokinetic decontamination technology. Electro-osmosis is the movement of a fluid due to an applied electric field relative to a stationary soil mass. Predominantly fluid migration is from the anode to the cathode due to the negatively charged soil surface. The second mechanism, ionic migration, is the movement of ions in the pore solution under the influence of an electric field. Positive ions (cations) migrate towards the cathode while negative ions (anions) are transported towards the anode. In cases where the soil zeta potential is small contaminant transport occurs mainly by electromigration [3,4].

Fundamental explanations of conduction processes in the soil under electrical and hydraulic potentials have recently been proposed [3–12]. Acar et al. [6] have studied the pH distributions and their role in contaminant decontamination. Jacobs et al. [3] have developed a mathematical model to simulate metal removal under applied electric fields.

Chromium, is an important heavy metal pollutant arising from many diverse fields such as metallurgy, electroplating, leather tanning, chemical catalysts, pigments, corrosion inhibitors, printing inks, etc. Chromium is a transition element with oxidation states from 0 to 6^+ but mainly exists in the environment as Cr(III) or Cr(VI). Hexavalent chromium [Cr(VI)] is both toxic and mutagenic. Trivalent chromium [Cr(III)] is the most stable form, but is very insoluble and hence aqueous concentrations are well below water quality standards [13]. The Cr(VI) state is generally considered to pose the greatest health risk because it is toxic, more mobile and easily soluble. Cr(VI) has high solubility in water and exists as chromate ($CrO4^{2-}$), monochromate ($HCrO4^{-}$) or dichromate ($Cr_2O_7^{2-}$) anions depending on the pH of the solution. This hexavalent chromium is the chemical form requiring disposal/remediation.

In this paper, the theoretical considerations underlying the successful decontamination of hexavalent chromate were investigated. The objective was to gain a better understanding of the process through modeling so that effective means can be taken to remediate the soil. The model predictions are compared with the experimental results from laboratory scale studies [14].

2. Experimental

The electrochemical cell employed for the decontamination feasibility studies was a cylindrical column 1.2 cm diameter and 80 cm long depicted in Fig. 1. The experiments were conducted using a Model NFB filtered d.c. power supply (EPSCO). ACS Reagent chemical was used to prepare a conducting electrolyte consisting of 40–80 mesh Ottawa

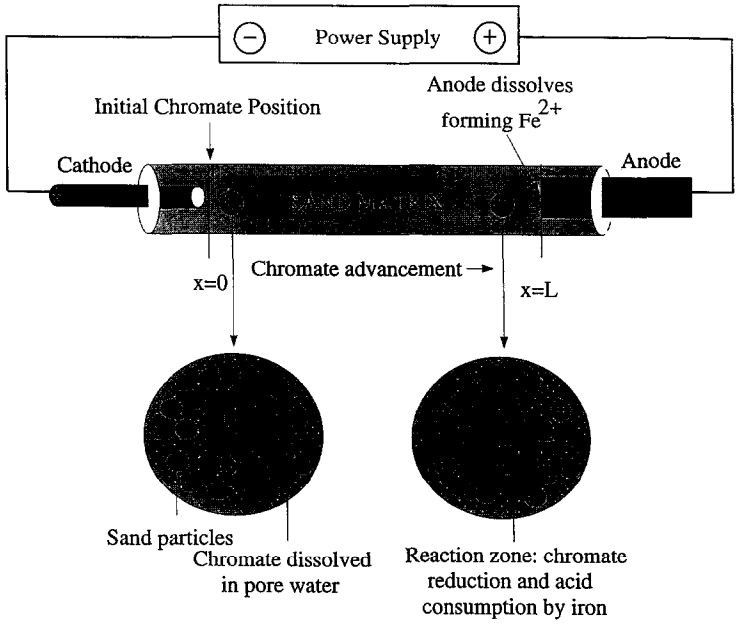

Fig. 1. Schematic of cylindrical cell for chromate decontamination studies.

sand and 8% Na_2SO_4 by weight. Four different sand samples with varying water contents of 12, 13.5, 15 and 17% were prepared. The saturated sand electrolyte was packed tightly in the column. Graphite served as the inert cathode while alpha pure 99.9% iron was used as the anode. The electrodes were placed on both sides of the soil column and connected to the constant voltage source. ACS grade fine potassium chromate dissolved in deionized water was kept close to the cathode in all the cells. A potential of 40 V was applied across the porous media in all the cells. Application of an electric field resulted in chromate movement from the cathode to the anode.

The feasibility of complete in-situ decontamination of chromate was investigated by bench scale experiments. A test cell (length = 26 cm, width = 12.4 cm and height = 12.5 cm), as shown in Fig. 2 was constructed. For the experiment, 4650 g of 40–60 mesh Ottawa with a water content of approximately 10% by weight was filled in the rectangular cell. Alfa pure 99.99 Fe was used as the anode while graphite electrodes served as the cathode. The sand sample was electrolyzed at a constant potential of 25 V. ACS grade reagent potassium chromate was loaded close to the cathode. The transport of chromate and the soil chemistry associated with the application of the potential gradient were studied. The hydrogen ion activity in the soil was measured periodically using a pH meter. The moisture content in the cell was maintained at the initial level by regular addition of water at the anode and cathode. This procedure was carried out in order to compensate for the depletion of water due to the water electrolysis reactions at the electrodes.

After a duration of one month when the chromate ions had advanced to the anode all the experiments were interrupted. The sand specimens were removed from the cell and

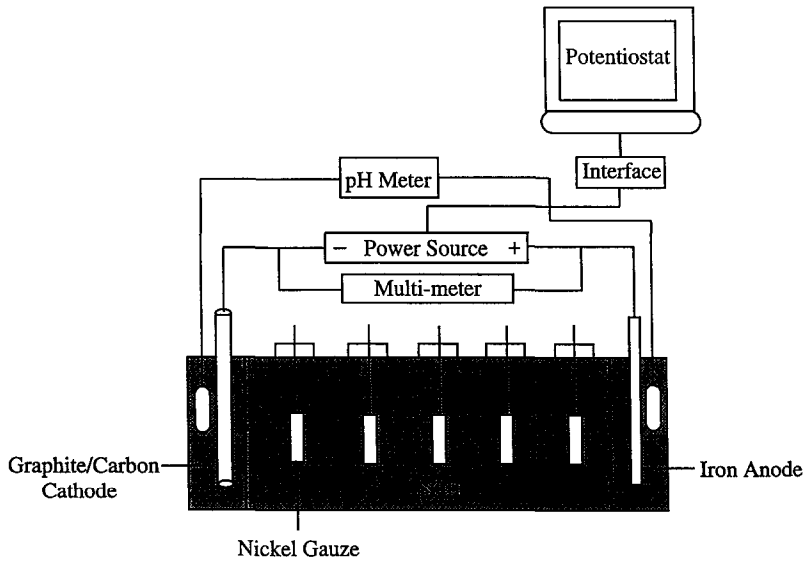

Fig. 2. A schematic diagram of the set-up for bench scale testing of electrokinetic remediation of chromate from sand.

cut into segments of 5 cm each. A known weight of the sand (2–5 mg) from each section was dissolved in a given volume of deionized water. The stock solution thus obtained was stirred for 20 min to allow the undissolved solid particles to settle. The supernatant obtained from each of the 16 stock solutions was analyzed for pH, total chromium and iron contents. Atomic absorption spectroscopy (AA) was done to determine the total chromium and iron present in each segment of the cell. For both chromium and iron the AA was calibrated initially using standard test solutions of Cr and Fe.

3. Theory

A schematic of the electrokinetic cell being modeled here is shown in Fig. 1. It consists of a graphite cathode and iron anode with sand of different water contents as the conducting electrolyte.

The assumptions involved in this model are as follows.

1. The behavior of the process can be described by a one-dimensional model.
2. Dilute solution theory applies [15]. To avoid the complexities associated with using concentrated solution theory, dilute solution theory was used. The interactions between the solutes are assumed to be negligible.
3. The Nernst-Einstein equation, $D_i^{\text{eff}} = u_i RT$, which is implicit in the dilute solution theory, applies here [15].
4. The electro-osmotic velocity is assumed to be zero for sand because of its very low surface charge and zeta potential.

5. The tortuous nature of the soil medium is accounted by the Macmullin number, which is given by the ratio of tortuosity to porosity of soil [16]. The effective diffusion coefficient of individual ions is given by the infinite solution diffusion coefficient divided by the Macmullin number.
6. The physical, transport and electrokinetic parameters are constant throughout the electrolyte medium.
7. No heterogeneous chemical reactions occur in the sand and the sorption processes can be approximated by the retardation factor [17]. Electrochemical reactions occur at the surface of the electrodes.
8. The cell is isothermal.

3.1. Governing equations

The model presented below includes the electrode reactions involving the production of H^+ and OH^- and the bulk water hydrolysis reactions. Mass transport in this system is due to migration in an electric field and diffusion in a concentration gradient. Therefore the flux expression for each species i can be written as

$$N_i = -\frac{D_i}{N_{mac}}\nabla c_i - z_i u_i F c_i F \nabla \Phi \tag{1}$$

where

$$N_{mac} = \frac{\tau}{\epsilon} \tag{2}$$

The tortuosity, τ, is a measure of the effect of the shape of the flowpath followed by different species in a porous media. The time rate of change in concentration of a given species i is

$$\frac{\partial \epsilon c_i}{\partial t} = -\nabla \cdot N_i + R_{sor} + R_{rxn} \tag{3}$$

R_{sor} is the rate at which the species is adsorbed/absorbed on the surface of the porous medium and R_{rxn} is the rate at which the species is depleted or formed due to chemical reactions in the bulk phase. By combining Eq. (1) and Eq. (3), we obtain the following equation for one spatial coordinate:

$$\frac{\partial \epsilon c_i}{\partial t} = \frac{D_i}{N_{mac}}\frac{\partial^2 c_i}{\partial x^2} + u_i z_i F c_i \frac{\partial^2 \Phi}{\partial x^2} + u_i z_i F \frac{\partial c_i}{\partial x}\frac{\partial \Phi}{\partial x} + R_{sor} + R_{rxn} \tag{4}$$

Sorption processes include chemisorption, absorption, adsorption and ion exchange. The sorption processes are determined by assuming equilibrium conditions and applying the conditions of equilibrium sorption isotherm. For a direct relationship between the amount of solute sorbed onto unit weight of solid, c_i^*, and the concentration of the solute, c_i, the adsorption isotherm of c_i as a function of c_i^* is given by the equation:

$$c_i^* = K_d c_i \tag{5}$$

where K_d is a constant known as the distribution coefficient [17]. The distribution coefficient is the ratio between the amount of contaminant adsorbed onto the solid

surfaces to the concentration of contaminant in the pore fluid. The sorption reaction rate is given by

$$R_{\text{sor}} = -\rho \frac{\partial c_i^*}{\partial t} \tag{6}$$

where ρ is the density of the soil. Substituting for the sorption reaction term, we have the change in concentration of species i:

$$\frac{\partial \epsilon c_i}{\partial t} = \frac{D_i}{N_{\text{mac}}} \frac{\partial^2 c_i}{\partial x^2} + u_i z_i F c_i \frac{\partial^2 \Phi}{\partial x^2} + u_i z_i F \frac{\partial c_i}{\partial x} \frac{\partial \Phi}{\partial x} - \rho \frac{\partial c_i^*}{\partial t} + R_{\text{rxn}} \tag{7}$$

This can be reorganized as

$$\frac{\partial \epsilon c_i}{\partial t} Rd_i = \frac{D_i}{N_{\text{mac}}} \frac{\partial^2 c_i}{\partial x^2} + u_i z_i F c_i \frac{\partial^2 \Phi}{\partial x^2} + u_i z_i F \frac{\partial c_i}{\partial x} \frac{\partial \Phi}{\partial x} + R_{\text{rxn}} \tag{8}$$

What has been termed the retardation factor, Rd_i, is given by

$$Rd_i = 1 + \frac{\rho}{\epsilon} K_{\text{d}} \tag{9}$$

In this model chromate is assumed not to take part in any chemical reactions. The only chemical reaction in the bulk is the water hydrolysis reaction:

$$H_2O \leftrightarrow H^+ + OH^- \tag{10}$$

Since the rate of reactions of H^+ and OH^- are equal subtracting the transport Eq. (8) for OH^- from that of H^+ gives

$$\left(Rd_{H^+} \frac{\partial \epsilon c_{H^+}}{\partial t} - Rd_{OH^-} \frac{\partial \epsilon c_{OH^-}}{\partial t} \right)$$
$$= \frac{D_{H^+}}{N_{\text{mac}}} \frac{\partial^2 c_{H^+}}{\partial x^2} - \frac{D_{OH^-}}{N_{\text{mac}}} \frac{\partial^2 c_{OH^-}}{\partial x^2} + u_{H^+} z_{H^+} F c_{H^+} \frac{\partial^2 \Phi}{\partial x^2} - u_{OH^-} z_{OH^-} F c_{OH^-} \frac{\partial^2 \Phi}{\partial x^2}$$
$$+ u_{H^+} z_{H^+} F \frac{\partial c_{H^+}}{\partial x} \frac{\partial \Phi}{\partial x} - u_{OH^-} z_{OH^-} F \frac{\partial c_{OH^-}}{\partial x} \frac{\partial \Phi}{\partial x} \tag{11}$$

From the mass equilibrium for the water ionization reaction we have for OH^-:

$$c_{H^+} c_{OH^-} = K_{\text{w}} \tag{12}$$

For the rest of the species CrO_4^{2-}, K^+, Na^+ and SO_4^{2-} the transport equation is as follows

$$\frac{\partial \epsilon c_i}{\partial t} Rd_i = \frac{D_i}{N_{\text{mac}}} \frac{\partial^2 c_i}{\partial x^2} + u_i z_i F c_i \frac{\partial^2 \Phi}{\partial x^2} + u_i z_i F \frac{\partial c_i}{\partial x} \frac{\partial \Phi}{\partial x} \tag{13}$$

Since the net charge in the bulk electrolyte is zero, the equation of electroneutrality

$$\Sigma z_i c_i = 0 \tag{14}$$

holds good in the soil. This constraint is used to calculate the potential in the soil. Electroneutrality is observed in all solutions except in a thin double layer near the

electrodes. This double layer is of the order of 1–10 nm in thickness [15]. A more appropriate equation which considers the double layer effects is the Poisson's equation. For a medium of uniform dielectric constant, ψ, [15],

$$\nabla^2 \Phi = \frac{F}{\varphi} \sum_i z_i c_i \tag{15}$$

The value of the proportionality constant (F/ψ) is very large $(1392 \times 10^{16}$ for a relative dielectric constant of 78.303) so that an appreciable separation of charge would require prohibitively large electric forces. The close adherence of soil media to Eq. (14) and also the mathematical simplification arising from this justifies the use of the electroneutrality condition for calculating the potential at all regions in the electrolyte. However, the application of electroneutrality does not imply that the Laplace's equation holds good for the potential.

3.2. Boundary conditions

To solve the governing equations given above appropriate boundary and initial conditions must be specified. Due to the water electrolysis reaction at the electrodes hydrogen ions are produced at the anode and hydroxyl ions are produced at the cathode and this is given by

$$\text{At } x = 0 \quad \frac{1}{2}H_2O - e^- \rightarrow \frac{1}{4}O_2 \uparrow + H^+ \tag{16}$$

$$\text{At } x = L \quad H_2O + e^- \rightarrow \frac{1}{2}H_2 \uparrow + OH^- \tag{17}$$

The production rate of H^+ at the anode is equivalent to the current passing through the soil,

$$-\frac{D_{H^+}}{N_{mac}} \frac{\partial c_{H^+}}{\partial x} - z_{H^+} u_{H^+} F c_{H^+} \frac{\partial \Phi}{\partial x} = \frac{i_1 \eta}{F\epsilon} \tag{18}$$

where i_1 is the anodic current density for Eq. (16) and η is the anode current efficiency. The anodic current density is given by the Butler-Volmer equation

$$i_1 = i_{o1,ref} \left\{ \exp\left[\frac{\alpha_{a1} F}{RT} (E_a - \Phi_{x=0} - E_{1,ref}) \right] - \left(\frac{c_{H^+}}{c_{H^+,ref}} \right) \times \exp\left[\frac{-\alpha_{c1} F}{RT} (E_a - \Phi_{x=0} - E_{1,ref}) \right] \right\} \tag{19}$$

where $i_{o1,ref}$ is the reference exchange current density for Eq. (16), E_a is the applied potential at the anode, α_{a1} and α_{c1} are the anodic and cathodic transfer coefficients for Eq. (16). $E_{1,ref}$ is the open-current potential of Eq. (16) at the reference concentrations and is given by

$$E_{1,ref} = E_1^\theta - E_{re}^\theta + \frac{RT}{F} \ln(c_{H^+,ref}) + \frac{RT}{n_{re} F} \sum s_{i,re} \ln(c_{i,re}) \tag{20}$$

where E_1^θ and E_{re}^θ are the standard half cell potentials for Eq. (16) and the reference electrode respectively. n_{re}, $c_{i,re}$ and $s_{i,re}$ denote the number of electrons, reference

concentrations of ionic species and the stoichiometric coefficients of these species associated with the reference electrode half cell reaction. The concentration of hydroxyl ions is given by the water ionization equilibrium Eq. (12). Similarly for hydroxyl ions at the cathode

$$-\frac{D_{OH^-}}{N_{mac}}\frac{\partial c_{OH^-}}{\partial x} - z_{OH^-}u_{OH^-}Fc_{OH^-}\frac{\partial \Phi}{\partial x} = \frac{i_2}{F\epsilon} \tag{21}$$

where

$$i_2 = i_{o2,ref}\left\{\left(\frac{c_{OH^-}}{c_{OH^-,ref}}\right)\exp\left[\frac{\alpha_{a2}F}{RT}(E_c - \Phi_{x=L} - E_{2,ref})\right] - \exp\left[\frac{-\alpha_{c2}F}{RT}(E_c - \Phi_{x=L} - E_{2,ref})\right]\right\} \tag{22}$$

where

$$E_{2,ref} = E_2^\theta - E_{re}^\theta - \frac{RT}{F}\ln(c_{OH^-,ref}) + \frac{RT}{n_{re}F}\Sigma s_{i,re}\ln(c_{i,re}) \tag{23}$$

The rest of the parameters have the same significance as discussed before for Eq. (19) and Eq. (20). For the purpose of convenience the equilibrium potentials for Eq. (16) and Eq. (17) were chosen to be relative to Eq. (16) [i.e. re = 1 in Eq. (20) and Eq. (23)]. It should be noted that the cell potential $(E_a - E_c)$ is actually the independent variable, not E_a. That is, even though E_a and E_c can be varied independently within the model, the results depend only on their difference, not their individual values. The hydrogen ion concentration is given by Eq. (12) at the cathode. For the rest of the species the flux is zero at both the anode and cathode.

$$-\frac{D_i}{N_{mac}}\frac{\partial c_i}{\partial x} - z_i u_i F c_i \frac{\partial \Phi}{\partial x} = 0 \tag{24}$$

The potential in the soil is given by the electroneutrality condition. At both $x = 0$ and $x = L$,

$$\sum z_i c_i = 0 \tag{25}$$

Since chromate is loaded only to a particular distance in the cell initially this is expressed mathematically as

$$c_{CrO_4^{2-}} = c_{CrO_4^{2-},ref} \quad x < \delta$$

$$c_{CrO_4^{2-}} = 0 \qquad x \geq \delta$$

where δ is the distance to which chromate is initially placed in the cell. For the rest of the species the initial conditions are simply that

$$t = 0 \; c_i = c_{i,ref} \tag{27}$$

By subtracting Eq. (8) for OH^- from that of H^+ the concentration of OH^- has been introduced in Eq. (11). An additional equation which describes the concentration of OH^- is given by the mass equilibrium for the water ionization reaction in Eq. (12). Eq. (11) and Eq. (12) are coupled through the concentration terms for H^+ and OH^-. The

governing equations for all the species are coupled through the potential gradient. Eqs. (11)–(14) are the governing equations for seven variables namely, the six species and the potential. Since there are seven unknowns and seven dependent variables the system is well defined. It should be noted that Eq. (11) cannot be solved in isolation because of its coupled nature. Eqs. (11)–(14) constitute a set of coupled non-linear partial differential equations which are difficult to solve.

The numerical methodology consists of transforming the sets of coupled partial differential equations (PDEs) into sets of coupled ordinary differential equations (ODEs). A finite difference approximation accurate to $O^{(\Delta x)^2}$ where Δx is the largest step-size in the x direction is used for the differential equations. The coupled ODEs are converted to non-linear algebraic equations by using implicit stepping accurate to $O(\Delta t)$ in the time domain. The resulting finite difference approximations have a banded matrix structure that can be solved by Newman's BAND(J) [15] algorithm. The non-linearity of the problem causes the elements of the banded matrix to be functions of the independent variables. The non-linear equations are solved from the known initial values of the variables by proper iteration with Newton-Raphson. Due to the steepness associated with the pH gradients, minute resolution is needed in the spatial and temporal directions to get convergence.

The parameters used in the calculations were chosen to correspond to the experimental conditions. The values for tortuosity [17,18] and porosity [11,18,19] of sand were taken from literature. The anodic current efficiency was determined experimentally [14]. The free stream diffusion coefficient values for all ionic species were taken from Newman [15]. The initial concentrations correspond to the experimental conditions maintained. The retardation factor values used were chosen to correspond closely to those previously used by Alshawabkeh et al. [5] and also experimentally determined by Shackleford et al. [19]. The exchange current densities were chosen arbitrarily. The transfer coefficients for both reactions were assumed to be symmetric. The simulated results are presented and discussed next.

4. Model results

The model presented above can be used to predict the concentration of the individual species at various segments of the cell as a function of time. The model was tested for different water contents by changing the reference concentrations, porosity, tortuosity, applied current and retardation factor. The parameters used for 10, 12 and 13.5% water contents are given in Table 1. Significant results obtained are the pH and chromium concentrations as a function of time and distance. These results are compared to the experimental data on chromate decontamination [14].

4.1. pH profiles

The steady state in-situ pH profile for 17% water content as a function of distance from cathode is plotted in Fig. 3. Water electrolysis reactions at both the electrodes results in sharp pH gradients. H^+ and OH^- ions are generated at the anode and cathode respectively due to electrochemical reactions. The pH at the cathode increases sharply and that at the anode decreases. The two newly formed species interact with the

Table 1
Parameters used in numerical modeling

Porosity, ϵ				0.1–0.3
Tortuosity, τ				0.7
Applied potential, $(V_a - V_c)$ (V)				40
Electro-osmotic velocity (cm/s)				0
Faraday's constant (C/mol)				96487
Temperature (K)				298
Water equilibrium constant, K_w (mol^2/cm^6)				10^{-20}
Iron dissolution current efficiency, η				30%
Exchange current density for reactions (Eq. (16)) and (Eq. (17)), $i_{oj,ref}$ (A/cm^2)				10^{-5}
Transfer coefficient, α_{aj} and α_{cj}				0.5
Standard cell potential for reaction (Eq. (16)), $E_{1,ref}$ (V)				1.229
Standard cell potential for reaction (Eq. (17)), $E_{2,ref}$ (V)				0.401
Species	D_i (cm^2/s)	Rd_i	z_i	$c_{i,ref}$ (mol/cm^3)
H^+	93.1×10^{-6}	20	+1	10^{-10}
OH^-	52.8×10^{-6}	1	−1	10^{-10}
CrO_4^{2-}	1.070×10^{-5}	1	−2	$0.29–1.5\times10^{-3}$
K^+	1.957×10^{-5}	23	+1	$0.58–2.8\times10^{-3}$
Na^+	1.334×10^{-5}	28	+1	$0.107–0.17\times10^{-3}$
SO_4^{2-}	1.065×10^{-5}	1	−2	$0.054–0.085\times10^{-3}$

pollutants in solution and have a significant influence on the transport and fixation of contaminants. The sharp pH gradients have been observed in many electro-kinetic experiments [1,5–8]. An alkaline front sweeps across the cell up to the anode. Due to their ionic charges, hydroxyl ions are transported towards the anode and hydrogen ions towards the cathode. However the acid front is confined to a region adjacent to the anode because of the lower anodic current efficiency and also due to consumption by the iron anode. The model predicts the sweep of the hydroxyl ions through the column as time proceeds. As can be seen from the plot, the model also predicts the distance (65–70 cm from the cathode) to which the alkaline front has expanded in the cell.

The water equilibrium reaction plane between hydroxyl and hydrogen ions varies position with time. As seen in Fig. 3, a sharp variation in pH is observed at the reaction plane. After 350 h of electrolysis the reaction plane is fixed adjacent to the positive electrode. The abrupt change in pH near the anode is accompanied by the chemical reaction between the acid and alkaline fronts. In conventional electrokinetics, the movement of hydroxyl towards the anode due to diffusion is retarded by the counterflow due to electro-osmosis [5]. In this case electro-osmosis is negligible and no fluid flow from the anode to the cathode is seen. The pH at the anode depends on the rate of the hydrogen consumption reaction and the current density applied. The anodic current density is less because of the larger anode area compared to the cathode and also due to the iron dissolution reaction. The entire current applied at the negative electrode is spent on the generation of hydroxyl ions. Hence pH increases beyond 14 at the cathode. However at the positive electrode dissolution of the iron anode occurs concurrently with the production of hydrogen ions. A significant amount of the current is taken by this reaction. As seen from the plot, the pH at the anode remains at a low value after a

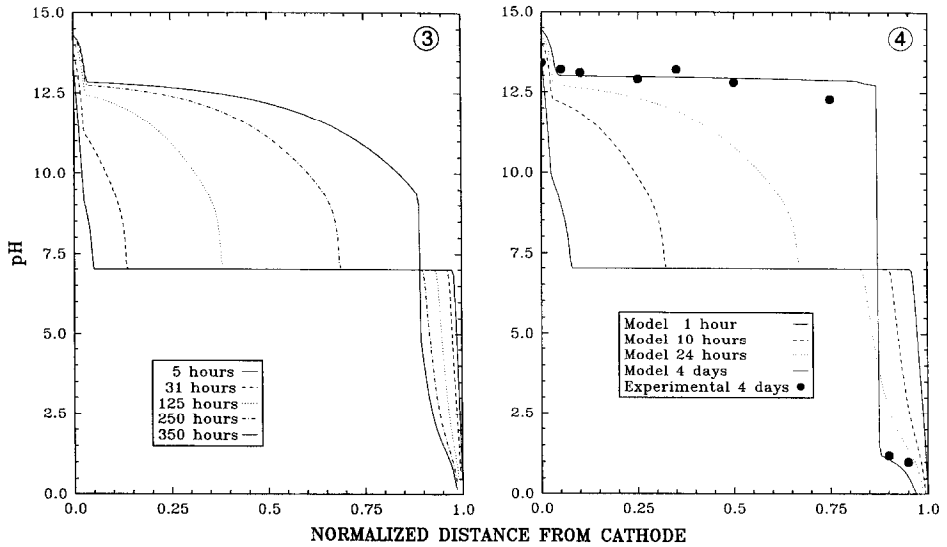

Fig. 3. Advancement of alkaline front as a function of time and distance for 17% water content.

Fig. 4. pH distribution in the rectangular cell. Comparison of model with experiment after 4 days.

certain period of electrolysis, which favors the reduction of hexavalent chromium to trivalent form by Fe^{2+}. Fig. 4 compares the pH after 4 days of electrolysis in the rectangular cell. Depending on the pH Cr(VI) exists in three different forms namely, CrO_4^{2-}, $HCrO_4^-$ and $Cr_2O_7^{2-}$. In basic solutions above pH 6.5 the yellow chromate ion CrO_4^{2-} is prevalent and in acidic solutions below pH 6, $HCrO_4^-$ and $Cr_2O_7^{2-}$ are the main species. Under acidic conditions and Cr(VI) concentrations greater than 10 mM, $HCrO_4^-$ polymerizes to the orange red dichromate ion $Cr_2O_7^{2-}$. The existence of the orange-red dichromate species at low pH values was seen experimentally for the cell with 17% water content close to the anode where sufficient Fe^{2+} was not present for the reduction process. However all the experiments were interrupted once the chromate front reached the low pH zone. The presence of iron was detected only in the region close to the anode both visually and also by AA spectroscopy. Hence the assumption that chromate ions do not react is valid within the experimental conditions maintained.

4.2. Concentration profiles

Figs. 5 and 6 present the time dependent variation of chromium concentration inside the cylindrical column. The reference concentrations and other parameters used in the model are listed in Table 1. In Fig. 5 the chromium concentration inside the column after a time period of 28 days is compared to the experimental results for 17% water content. The cell is initially loaded with a known amount of potassium chromate at the cathode. The chromate anions because of their negative charge migrate towards the anode due to the applied potential of 40 V. Since the column is sealed at both ends the

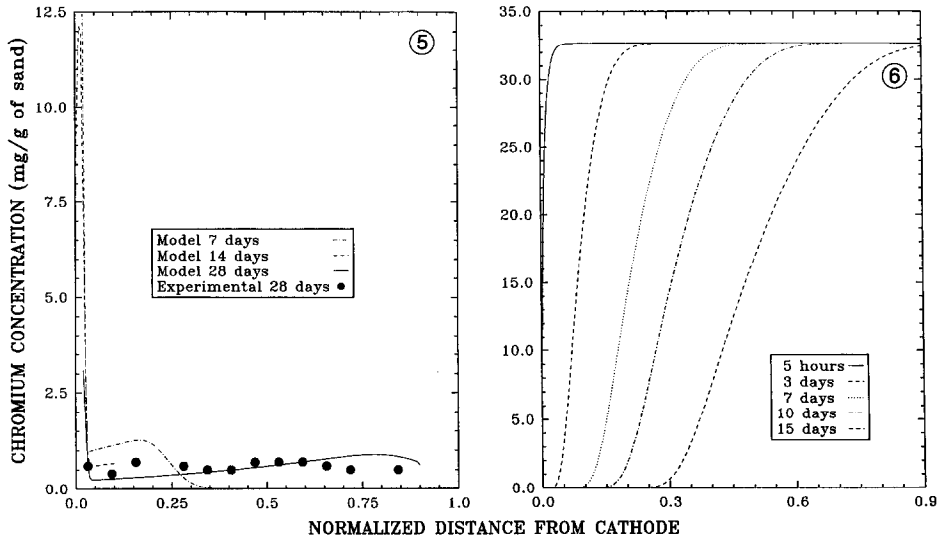

Fig. 5. Comparison of chromium concentration profile at the end of test period of 28 days for 17% water content.

Fig. 6. Chromium concentration profiles with uniformly loaded contaminant inside the cylindrical column.

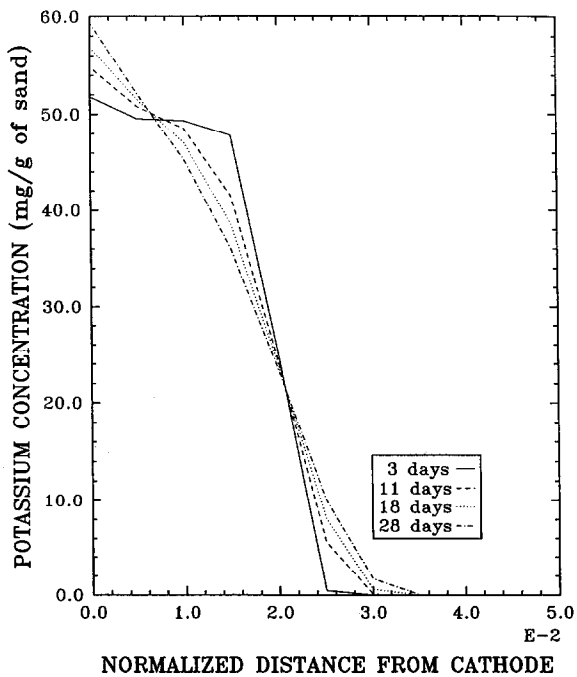

Fig. 7. Potassium ion profile inside the cylindrical column at different times.

chromate remains inside the tube only. As the water content varies the pore structure of sand changes resulting in changes in the physical parameters. Good agreement is seen between the experimental and model results. Fig. 6 presents the chromium concentration profiles with a uniform contaminant loading throughout the cell. As time increases the entire amount of chromate is accumulated at the anode where it undergoes reduction.

The potassium concentration profiles are presented in Fig. 7 to demonstrate the dominance of ionic migration over other transport mechanisms. The potassium cations are positively charged and hence remain at the cathode where they had been placed initially. No transport of potassium beyond a small region adjacent to the anode is seen. Hence it can be concluded that electromigration controls the entire process at very high potential gradients.

5. Summary and conclusions

Experimental studies have been conducted to examine the effect of ionic migration in the transport and subsequent in-situ fixation of chromate in sand [14]. A mathematical model for the entire process was developed which describes the physical processes involved. The good agreement between the model and the data demonstrates that the analysis is likely to be an accurate estimate of the physical situation, within the limits of the assumptions made. The combined effects of activation, mass transfer and ohmic polarization have been included in the model. The effect of pH distributions on the overall process has been demonstrated by the experimental results [14] and the model predictions here, as well as the model and empirical data of Shapiro et al. [7,8] and Acar et al. [6,20–22]. The numerical model correctly predicts the sweep of the alkaline front across the sand matrix due to the movement of the OH^- ions. In response to the generation of pH gradients the chemistry of the decontamination process is altered significantly. The water electrolysis reaction at both electrodes, the sorption processes in sand and the water hydrolysis reaction have been included in the model. Concentration profiles for the movement of ionic species under a potential field are simulated for different times. Comparison of the chromate concentration profiles in the cell after 28 days of electrolysis with experimental data yields good agreement. The models presented here may serve as a basis for simulating the behavior of electrokinetic cells based on ionic migration. If physical data are available, utilizing a model described herein could be a cost-effective way to choose optimum conditions for further study. The model could also be useful in evaluating further possible refinements to this decontamination process, such as uniform mixing of contaminants in sand and different flow patterns like electro-osmosis and convection for other types of soil (clay).

6. List of symbols

c_i concentration of species i (mol cm^{-3})
$c_{i,ref}$ reference concentration of species i (mol cm^{-3})
c_i^* amount of solute sorbed per unit weight of soil (mol kg^{-1})

D_i^{eff} effective diffusion coefficient of species i ($\text{cm}^2\ \text{s}^{-1}$)
E_a potential at the anode (V)
E_c potential at the cathode (V)
$E_{j,\text{ref}}$ open-current potential of reaction j (V)
E_j standard half cell potential of reaction j (V)
F Faraday's constant (96 487 C mol^{-1})
i_j current density for reaction j (A/cm^2)
$i_{oj,\text{ref}}$ reference exchange current density for reaction j (A/cm^2)
K_d distribution coefficient in adsorption isotherm ($\text{cm}^3\ \text{kg}^{-1}$)
K_w water dissociation constant ($\text{mol}^2\ \text{cm}^{-6}$)
L length of the cylindrical cell (cm)
n_{re} number of electrons associated with the reference electrode half cell
N_i total flux of species i (moles $\text{cm}^{-2}\ \text{s}^{-1}$)
N_{mac} Macmullin number, ratio of the specific resistivity of sand saturated with water to the specific resistivity of water
R universal gas constant (8.3143 J $\text{kg}^{-1}\ \text{K}^{-1}$)
R_{rxn} rate of chemical reactions (mol $\text{cm}^{-3}\ \text{s}^{-1}$)
R_{sor} rate of sorption reactions (mol $\text{cm}^{-3}\ \text{s}^{-1}$)
Rd_i retardation factor of species i
$s_{i,re}$ stoichiometric coefficient of species in the reference electrode half cell
t time (s)
T temperature (K)
u_i mobility of ionic species i ($\text{cm}^2\ \text{mol}\ \text{J}^{-1}\ \text{s}^{-1}$)
x normal spatial coordinate (cm)
z_i charge of species i

Greek Symbols

α_{aj} anodic transfer coefficient for reaction j
α_{cj} cathodic transfer coefficient for reaction j
ϵ porosity of sand
η anode current efficiency
ρ density of sand (kg cm^{-3})
τ tortuosity of sand
Φ potential in the soil (V)
ψ permittivity or dielectric constant (F/cm)

Acknowledgements

This work was funded under the Westinghouse Savannah River Company Environmental Restoration Division through the South Carolina Universities Research and Education Task Order 125. The information contained in this article was developed in the course of work performed under Contract Number DE-AC09–88SR18035 with the US Department of Energy.

References

[1] Y.B. Acar, A.N. Alshawabkeh, Principles of electrokinetic remediation, Environ. Sci. Technol. 27 (13) (1993) 2638–2647.
[2] R. Lageman, Electroreclamation: application in the Netherlands, Environ. Sci. Technol. 27 (13) (1993) 2648–2650.
[3] R.A. Jacobs, M.Z. Sengun, R.E. Hicks, R.F. Probstein, Model and experiments on soil remediation by electric fields, J. Environ. Sci. Health A29 (9) (1994) 1933–1955.
[4] E.R. Hicks, S. Tondorf, Electrorestoration of metal contaminated soils, Environ. Sci. Technol. 28 (1994) 2203–2210.
[5] A.N. Alshawabkeh, Y.B. Acar, Removal of contaminants from soils by electrokinetics: A theoretical treatise, J. Environ. Sci. Health A27 (7) (1992) 1835–1861.
[6] Y.B. Acar, R.J. Gale, G.A. Putnam, J. Hamed, R.L. Wong, Electrochemical processing of soils: theory of ph gradient development by diffusion, migration and linear convection, J. Environ. Sci. Health A25 (6) (1990) 687–715.
[7] A.P. Shapiro, Electroosmotic purging of contaminants from saturated soils, Ph.D. Dissertation, MIT, Cambridge, MA 1990.
[8] A.P. Shapiro, R.F. Probstein, Removal of contaminants from saturated clay by electroosmosis, Environ. Sci. Technol. 27 (2) (1993) 283–291.
[9] J. Hamed, Y.B. Acar, R.J. Gale, Pb(II) removal from kaolinite by electrokinetics, ASCE-J. Geotech. Eng. 117 (2) (1991) 241–271.
[10] A.P. Shapiro, P.C. Renaud, R.F. Probstein, Preliminary studies on the removal of chemical species from saturated porous media by electroosmosis, PCH, PhysicoChem. Hydrodyn. 11 (5) (1989) 785–802.
[11] J.K. Mitchell, Fundamentals of Soil Behaviour, 2nd ed., Wiley, New York, 1993, pp. 228-285.
[12] G.R. Eykholt, D.E. Daniel, Impact of system chemistry on electroosmosis in contaminated soil, ASCE-J. Geotech. Eng. 120 (5) (1994) 797–815.
[13] L.D. Anderson, D.B. Kent, J.A. Davis, Batch Experiments characterizing the reduction of Cr(VI) using suboxic material from a mildly reducing sand and gravel aquifer, Environ. Sci. Technol. 28 (1) (1994) 178–185.
[14] B.S. Haran, B.N. Popov, G. Zheng, R.E. White, Development of a new electrokinetic technique for decontamination of hexavalent chromium from low surface charged soils, Env. Progress. 15 (3) (1996) 166–172.
[15] J.S. Newman, Electrochemical Systems, 2nd ed., Prentice-Hall, New Jersey, 1991.
[16] R.E. White, J.S. Beckerdite, J. Van Zee, in: R.E. White (Ed.), Electrochemical Cell Design, Plenum Press, New York, 1984 pp. 25-60.
[17] C.W. Fetter, Contaminant Hydrogeology, Wiley, New York, 1993.
[18] C.D. Shackleford, D.E. Daniel, Diffusion in saturated soil. I: Background, ASCE-J. Geotech. Eng. 117 (3) (1991) 467–484.
[19] C.D. Shackleford, D.E. Daniel, Diffusion in saturated soil. II: Results for compacted clay, ASCE-J. Geotech. Eng. 117 (3) (1991) 467–484.
[20] Y.B. Acar, A.N. Alshawabkeh, R.J. Gale, Fundamentals of extracting species from soils by electrokinetics, Waste Manage. 12 (3) (1993) 141–151.
[21] Y.B. Acar, H. Li, R.J. Gale, Phenol removal from kaolinite by electrokinetics, ASCE-J. Geotech. Eng. 118 (11) (1992) 1837–1852.
[22] Y.B. Acar, J. Hamed, Electrokinetic soil processing in remediation/treatment: synthesis of available data, Bulletin of the Transportation Research, Record No. 1312, Soils Geology and Foundations, Geotechnical Engineering, (1991) 152-161.